Chemical Physics Letters 856 (2024) 141634

Contents lists available at ScienceDirect

Chemical Physics Letters

journal homepage: www.elsevier.com/locate/cplett

Research paper

Oxygen plasma activated Au-assisted mechanical exfoliation for large-area, high-quality metal phosphorus trichalcogenides flakes

Mouhui Yan [a,b], Haotian Wang [a,1], Guanghui Cao [a,1], Wei Ren [a,*]

[a] State Key Laboratory of Advanced Special Steel & School of Materials Science and Engineering, International Center of Quantum and Molecular Structures, Department of Physics, Shanghai University, 99 Shangda Road, 200444, Shanghai, PR China

[b] Center for Semiconductor Heterogeneous Materials and Devices, Songshan Lake Materials Laboratory, Dongguan, 523830, Guangdong, PR China

HIGHLIGHTS

- The modified Au-assisted exfoliation method for large-area MPX_3 flakes.
- The reactivation mechanism of Au surface via oxygen plasma treatment.
- The chemical and structural stability of ultrathin MPX_3 as well as the Au/1L MPX_3 interaction are revealed.

GRAPHICAL ABSTRACT

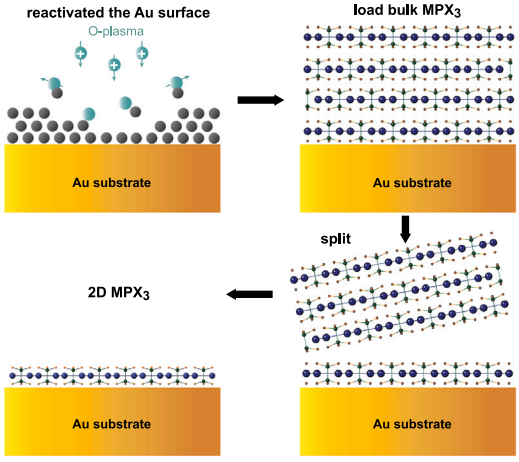

ARTICLE INFO

Keywords:
O-plasma
Au-assisted mechanical exfoliation
Trichalcogenides

ABSTRACT

The Au-assisted exfoliation method represents an advanced technique among mechanical exfoliation methods. However, the extensive constraints associated with the exfoliation process curtail the broader adoption and application of this technique. Here, we introduce a mild oxygen plasma process to reactivated the Au substrate, thereby addressing environmental-induced metal substrate failures and enabling the exfoliation of ultrathin flakes from layered $CoPS_3$ and $MnPS_3$. The obtained flakes measure up to several hundred microns and demonstrate high quality, as revealed by AFM, XPS, and Raman. This modified approach effectively enhance the practicality of the type of exfoliation method employing a metal film as tape.

1. Introduction

Two-dimensional (2D) materials are one of the most widely studied classes of materials. Several decades ago, Frindt [1] showed that atomically thin layers produced from van der Waals solids, a layered structure material with naturally single-atom-thick or polyhedral-thick layers, can be considered as an ideal 2D materials system. In 2004, Novoselov and Geim pioneered the discovery of graphene via mechanical exfoliation, demonstrating that layers of atoms derived from

* Corresponding author.
E-mail address: renwei@shu.edu.cn (W. Ren).
[1] These authors contributed equally to the work.

https://doi.org/10.1016/j.cplett.2024.141634
Received 12 May 2024; Received in revised form 30 August 2024; Accepted 11 September 2024
Available online 14 September 2024

van der Waals solids can be maintained in a stable state and exhibit unique physical properties [2]. Consequently, the emergence of pure 2D materials, which confine charge, thermal and dimensional effects to a single plane, has attracted considerable attention from researchers, marking the advent of the 2D materials era [3]. To date, the field of 2D materials is advancing rapidly, with significant progress in a variety of 2D materials classes, including black phosphorus [4], h-BN [5], MXene [6], CrI_3[7], $Cr_2Ge_2Te_6$[8], transition metal dichalcogenides (TMDs, e.g., MoS_2, WS_2, WSe_2, NbS_2) [9] and others. The distinctive physicochemical properties manifested in their 2D forms provide unprecedented opportunities for a host of emerging applications, such as low-dimensional confined catalysis [10], 2D superconductivity [11], new energy storage system [12], spintronics [13], and innovative electronic and optoelectronic devices [14,15]. Recently, a new class of multielement van der Waals materials, transition metal phosphorus trichalcogenides (MPT), has garnered increasing scientific interest [16,17]. The structural formula for MPT is denoted as MPX_3, where M represents a transition metal (Mn, Fe, Co, Ni, etc.), P is phosphorus, and X is chalcogen (S, Se, Te, etc.). From a crystallographic standpoint, MPT is structurally similar to TMDs (e.g., MoS_2), where one-third of the metal atoms are substituted by P-P dimers perpendicular to the layer, and these layers are systematically arranged into the $C2/m$ (X = S) or $R\bar{3}$ (X = Se) space groups, resulting in a 3D structure. Their inherent intralayer natural antiferromagnetism and wide bandgap range (1.2–3.5 eV, compared to 1.2–2 eV for TMDs) [18] significantly broaden the spectrum of applications for 2D materials in electronics, optoelectronics, and spintronics [19,20], establishing them as one of the focuses of research within the 2D materials domain.

However, obtaining high-quality 2D monolayers is a prerequisite for fundamental research on novel devices and diverse 2D properties. Notably, several methods have been reported as promising techniques for preparing 2D materials, such as chemical vapor deposition (CVD) [21,22], chemical exfoliation [23], and mechanical exfoliation [2,24]. Nevertheless, 2D samples synthesized via CVD present challenges in minimizing defects or grain boundaries [25], and the associated technical requirements are considerably high. In addition, surface contamination poses a obstacle for chemical exfoliation. For the research in high-performance devices as well as 2D electronics and magnetism, mechanical exfoliation method remains the preferred choice due to its simplicity and the superior quality of the obtained flakes [26]. With the development of mechanical exfoliation techniques, the inherent limitations to traditional tape methods, including small sample areas, low yield, and high randomness, have been largely overcome [27]. The gold-assisted exfoliation method [28] is one of the advanced universal mechanical exfoliation techniques, which can easily provide large-area, high-yield 2D samples. Subsequently, the exfoliated flakes can be transferred to other insulating substrates by etching out the Au film for a variety of applications [29]. Unfortunately, the limited allowable exposure time of the metal film to air (more than 6 min greatly reduces the probability of obtaining a monolayer sample) [30] and the high cost of the deposition process, constrain the practical application and promotion of this method.

In this study, we introduce a plasma-activated Au-assisted exfoliation technique, which employs a gentle plasma process for treating Au substrates exposed to atmospheric conditions for over a week, enabling the production of 2D MPX_3 samples up to several hundred microns, and provide an investigation of the exfoliation mechanism. Atomic force microscopy (AFM), X-ray photoelectron spectroscopy (XPS), and Raman spectroscopy are performed to reveal the effects of plasma treatment on the substrate and the quality of the obtained MPX_3 flakes. The results from argon and oxygen plasma treatments illustrate that the cleanliness, smoothness, and adhesion properties of the substrate significantly influence the efficacy of the exfoliation process. The finding shows that it is possible to reactivate a metal substrate as tape using a simple surface O_2 plasma treatment for high-quality, high-yield and large-area exfoliation of van der Waals materials. We believe that our process is effective in improving the limitations of metal-assisted exfoliation methods, reducing costs, and making the method more practical.

2. Experimental details

Layered $CoPS_3$ and $MnPS_3$ crystals were synthesized via a traditional chemical vapor transport (CVT) method [31]. The stoichiometric amounts of elements (metal: P: S = 1: 1: 3, 1 g in total) together with I_2 transport agent (about 50 mg) were vacuum-sealed into a quartz ampule and kept in a two-zone tube furnance for 7days. The temperature gradient for $CoPS_3$ and $MnPS_3$ are 600-500 °C and 780-730 °C, respectively. The Au substrates for mechanical exfoliation were prepared using an electron beam evaporation system (Ei-5z, ULVAC Inc.). Prior to deposition, 4-inch silicon wafers (Innotronix Technologies Co., Ltd) were ultrasonically cleaned with acetone, isopropanol (IPA) and deionized (DI) water, followed by blow-drying with a nitrogen gas gun. The ultimate vacuum of the deposition chamber is 2×10^{-3} Torr. A 10 nm Ti adhesion layer was deposited before 40 nm Au deposition. The deposition rates of Ti and Au are 1 and 0.5 Å/s, respectively. Subsequently, the gold-coated wafers were kept in ambient conditions for more than 7 days. The Au 'tape' for exfoliation was obtained by cutting the Ti/Au deposited Si wafers and then activated by a gentle plasma process (Triton40, Jet Plasma Co., Ltd). The Ar or O_2 plasma used to treat the surfaces was generated by applying 100 W radio frequency power under a 20 SCCM gas flow at partial pressure of 100 mTorr. Both plasma cleaning processes employ the same process parameters, only the gas is changed. Microscopic optical images were captured utilizing an MX8R microscope (Sunny Optical Technology Ltd.). The Surface morphology and roughness of the Au substrate before and after plasma treatment as well as the topography of obtained ultrathin flakes were evaluated by AFM scanning (Dimension Ican, Bruker) with Si tip (RTESPA-150) in tapping mode. XPS, using an Al Kα X-ray source (ESCALAB Xi+, Thermo Fisher), was employed to analyze the surface chemical states of the substrates and samples. The X-ray spot size ranges from 200 to 500 μm and Au $4f_{7/2}$ binding energy were used for the charge correction. Raman measurements were conducted on the LabRam HR Evolution system (Horiba Ltd.) using a 532 nm laser with a spot size of approximately 1 μm at room temperature. A low-energy laser of 53.2 μW and a high-resolution grating with a line density of 1800 gr/mm were selected for signal collection. Prior to each measurement, the Raman frequency was calibrated using the silicon Raman mode at 520 cm^{-1}.

3. Results and discussion

Fig. 1 shows the surface morphology and roughness of the Au substrates before and after the plasma treatment, acquired by AFM. The AFM images of the Au surface before plasma treatment and the 3D morphology of selected area (the white square region in Fig. 1(a)) are presented in Fig. 1(a) and (d), respectively. The raw Au substrate as shown in the inset of Fig. 1(a), a 4-inch Si wafer with 10 nm of Ti adhesion layer and 40 nm of Au layer, has a smooth surface with a surface roughness (R_q, root mean square deviation) of 0.74 nm. Ultrathin flakes can be identified on freshly prepared Au after exfoliation, as demonstrated in the lower left inset in Fig. 1(a). However, almost no flakes can be exfoliated after exposed to air more than seven days (see lower right inset in Fig. 1(a)). The Fig. 1(b) and (c) illustrate the AFM images after surface cleaning by O_2 and Ar plasma, respectively. The 3D morphology of the selected regions in Fig. 1(e) and (f) shows that the surface of the Au sample treated with O_2 plasma has a smoother surface with a roughness R_q of 0.54 than that of raw Au substrate, whereas the roughness of the Au substrate treated with Ar plasma under the same conditions increases significantly with a R_q of 2.04. As shown in the insets of Fig. 1(b) and (c), $CoPS_3$ flakes were mainly obtained from the Au substrate treated with O_2 plasma under the same process conditions (see also Fig. S1 in Supplementary materials for the exfoliation results with 9 min plasma treatment).

XPS analyses were conducted on gold substrates before and after plasma treatment to assess the effect of the gentle plasma treatment,

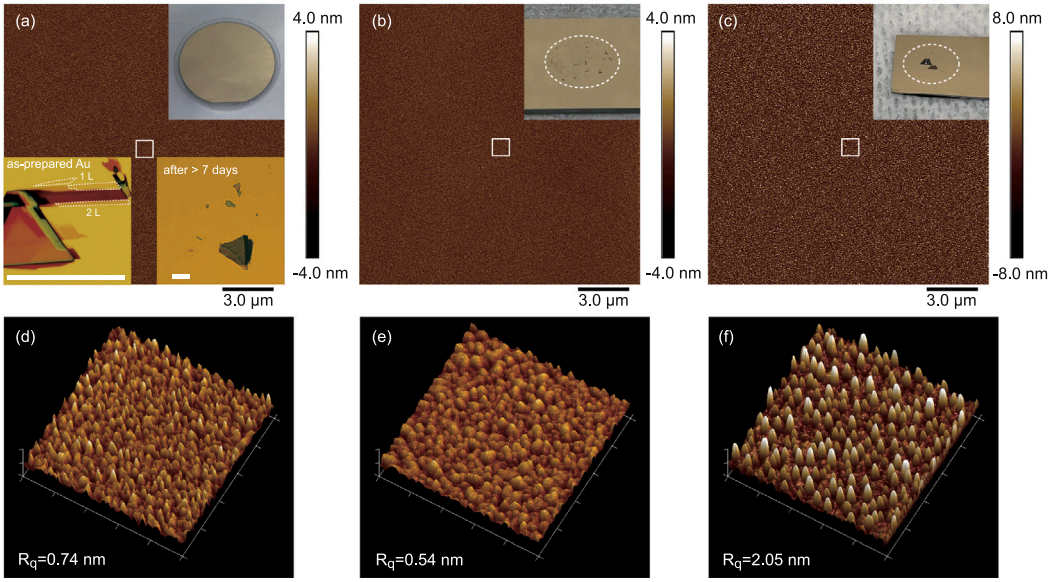

Fig. 1. AFM characterization of Au substrate before and after plasma: (a) the raw Au substrate (the upper right inset is a photo of the 4-inch wafer after Au/Ti deposition; the two insets below are optical microscope images of the exfoliation performed on the freshly prepared gold film and after 1 week of exposure to air, respectively; the white scale bar represents 40 μm), after 3 min (b) O_2 plasma and (c) Ar plasma treatment (the inset is optical image of the substrate after exfoliation). (d), (e) and (f) 3D AFM topography of the corresponding selected area (1 × 1 μm white square) in (a), (b) and (c), respectively.

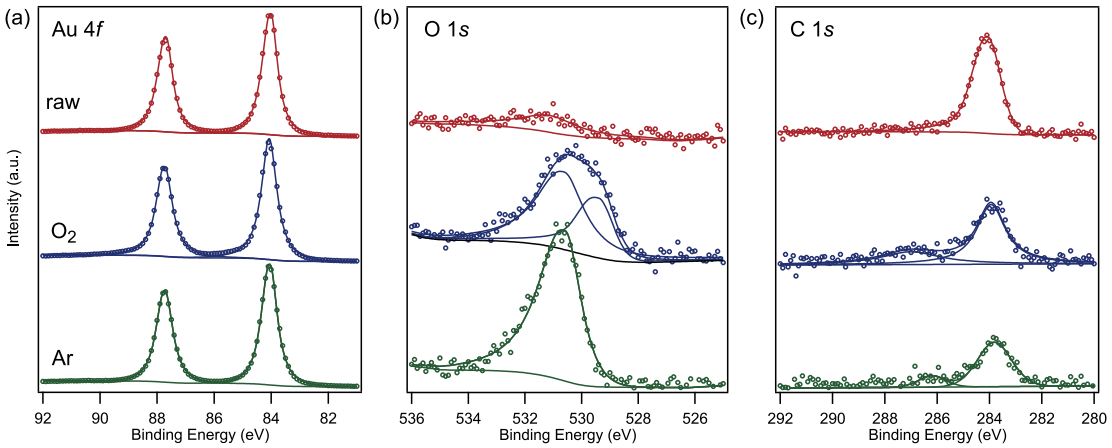

Fig. 2. XPS spectra of Au substrate before and after 3 min of gentle plasma treatment with oxygen or argon: (a) Au 4*f*, (b) O 1*s* and (c) C 1*s*.

as shown in Fig. 2. The peak intensities of the C 1*s* region and the O 1*s* region are standardized by the peak intensity of Au $4f_{7/2}$ for comparison. In O 1*s* region, the Au substrates received Ar and O_2 plasma treatment present more significant O-derived contamination (at 530.5 eV) from ambient environment. The reason for this is that the surface plasma treatment increased the interfacial adhesion strength of the Au substrate, which, in the case of the Ar plasma-treated Au substrate, is stronger than that of the O_2 plasma [32]. It should be noted that the O 1*s* peak on the low binding energy side of the oxygen plasma-treated Au substrate originates from Au_2O_3 [33]. No significant oxidation peaks were observed in the Au 4*f* region due to the low amount of oxidation. In C 1*s* region, carbon-derived signal is reduced by less than half because the plasma-treated Au substrate adsorbs carbon-containing gas molecules from the air. However, Ar plasma can physically etch the substrate surface by bombarding with Ar ions or atoms to remove all contaminants on the metal surface [34], which is also reflected in the surface morphology of the Ar-treated substrate in Fig. 1(f). Hence, the combination of the XPS results presented in Fig. 2(b, c) and the AFM results shown in Fig. 1(d, e, f) indicates that a gentle O_2 plasma process is effective in removing surface contamination via chemical reaction without damaging the surface structure or even reducing the surface roughness. In general, surface roughness and cleanness are the two main process parameter that affect the efficiency of Au-assisted exfoliation. It has been demonstrated that exfoliation efficiency notably increases as Au surface roughness decreases [30]. Therefore, O_2 plasma cleaning facilitates the acquisition of 2D samples by mechanical exfoliation [24,35].

Before mechanical exfoliation, the Au substrate, which has been kept in ambient atmosphere for more than 7 days, was ultrasonically cleaned in acetone, IPA and DI water, followed by 3 min of gentle oxygen plasma to remove adsorbates from the surface. The MPX_3 loaded blue tape was then brought into contact with the Au substrate as soon as possible and slight pressure was applied with a cotton bud to ensure uniform contact, the tape is removed after 2-5 min. The optical micrographs and corresponding AFM images of ultrathin $MnPS_3$ and $CoPS_3$ obtained by O_2 plasma treated Au substrate are shown in Fig. 3. Fig. 3(a) and (b) display typical $MnPS_3$ flakes prepared using the plasma-activated Au-assisted exfoliation method. The size of the monolayer can reach ~ 100 × 100 μm, and several ultrathin flakes can be observed within the field of view of the optical microscope

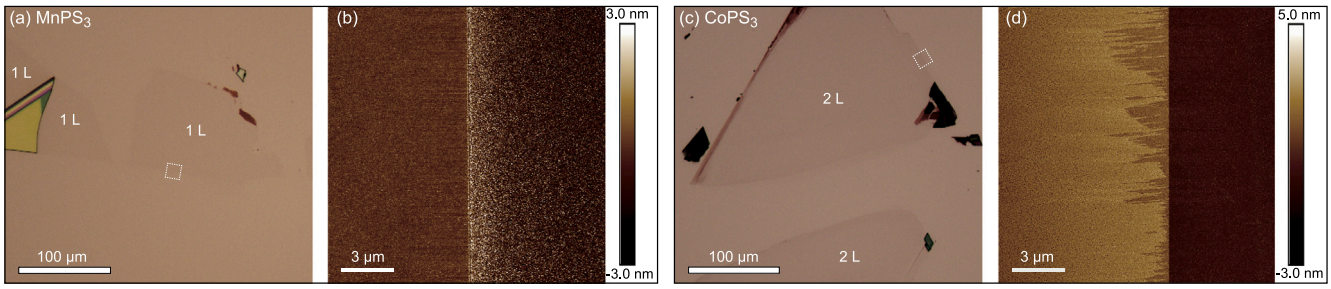

Fig. 3. Optical and AFM images of exfoliated $MnPS_3$ (a, b) and $CoPS_3$ (c, d).

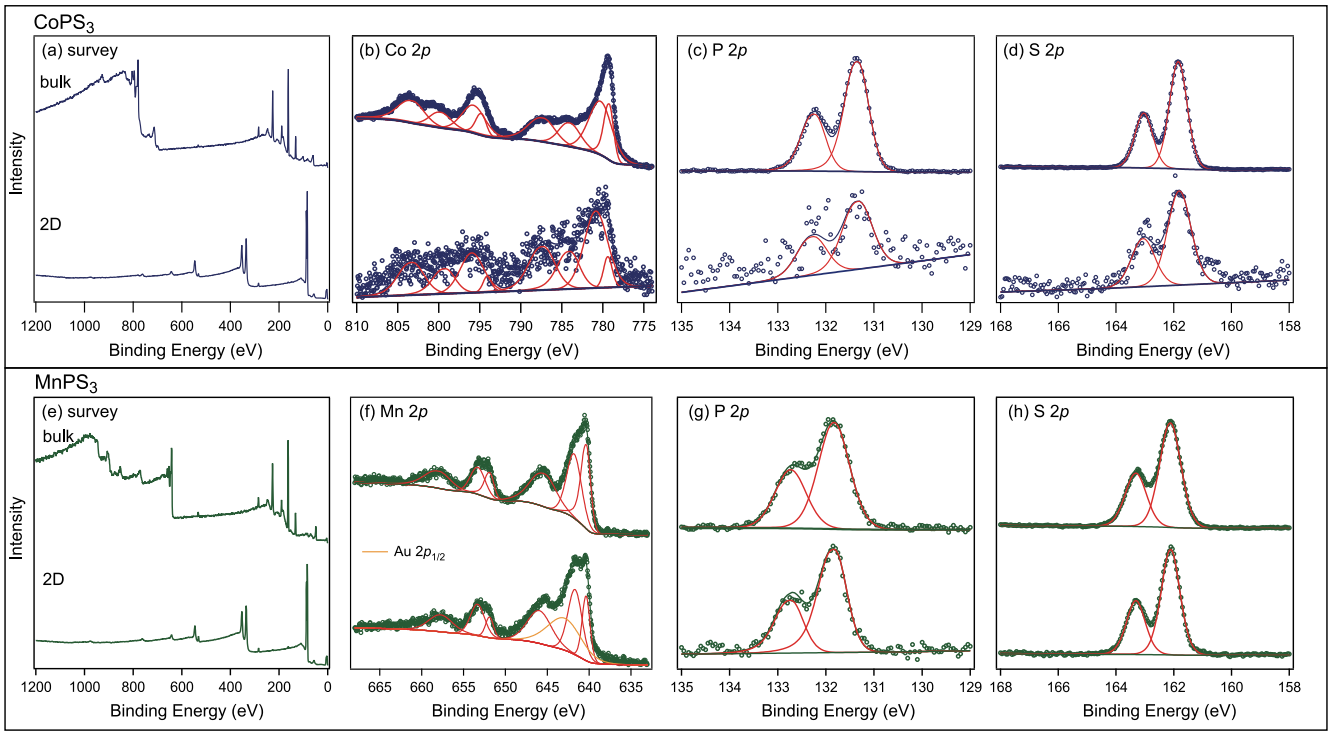

Fig. 4. Survey and core-level XPS spectra before and after exfoliated: (a-d) $CoPS_3$, (e-h) $MnPS_3$.

image. In addition, large-sized $CoPS_3$ ultra-thin films (~ 300 × 150 μm) can be obtained in the same step (Fig. 3(c, d)), indicating that this method may be applicable to MPX_3 type materials. The obtained flakes are significantly larger than the traditional exfoliated method previously reported for MPX_3 family [36]. One need to note that, the ultrathin MPX_3 flake are cleaved from a multilayer, not from the tape itself. The efficiency of exfoliation is determined by the competition of the forces between the sample layers and between the outermost layer and the substrate [28,37]. A sheet can only be separated from a multilayer and transferred onto the substrate when the force between the outermost sheet and the substrate exceeds that between the layers. Hence, exfoliating the sample too many times is not favorable for obtaining large sized samples due to the potential damage it can cause. Here, we cleaved the bulk sample only 4 to 6 times after attaching it to the blue tape. From the above results, it can be demonstrated that oxygen plasma treatment can effectively reactivate the Au substrate to easily obtain ultrathin large-area MPX_3 flakes due to the clean, smooth and somewhat adsorptive surface.

To confirm the effectiveness of this modified Au-assisted exfoliation method in providing structurally stable and chemically stable ultra-thin MPX_3 samples, detailed XPS analysis and Raman spectroscopy were performed on the samples before and after exfoliation. The chemical states of elements (Co 2*p*, Mn 2*p*, P 2*p*, S 2*p*) in the studied compounds are compiled in Fig. 4. The survey spectra of bulk $CoPS_3$ and $MnPS_3$ are consistent with previous work [38,39], demonstrating the correct proportions for all elements and can serve as a reference for exfoliated flakes. For the Co 2*p* characteristic lines, the peak shapes and positions of the bulk and ultrathin samples exhibit similarity, with Co $2p_{3/2}$ and Co $2p_{1/2}$ decomposed into four distinct components: the two main peaks (Co^{2+}, Co^{3+}) and two satellite peaks at higher binding energies corresponding to different final state with different screening mechanisms [40,41]. The fitting results for the Co 2*p* spectra reveal a slight increase in intensity of the Co^{3+} component at $E_B \approx 780.4$ eV in the 2D sample, which is also reflected in the increase of the intensity of the satellite peak, indicating the correlation between the charge state of the Co ion and the Au/$CoPS_3$ interaction. This phenomenon can be attributed to the substrate-induced charge doping [42]. In the case of Mn 2*p* characteristic lines, although the Au $2p_{1/2}$ peak signals of the substrate overlap with the Mn $2p_{3/2}$ peak signals, the chemical state of the Mn $2p_{1/2}$ portion demonstrate that there is also a relative enhancement of the Mn^{3+} peak at $E_B \approx 653.4$ eV of the exfoliated sample. As shown in Fig. 4 (c, d) and (g, h), the respective P 2*p* and S 2*p* spectra of $CoPS_3$ and $MnPS_3$ show clear spin–orbital splitting, indicating the stable chemical state of the ligand atoms in the $[P_2S_6]^{4+}$ unit.

In order to ascertain the crystallographic quality of the ultrathin MPX_3 flakes obtained, Raman spectroscopy using a 532 nm laser was

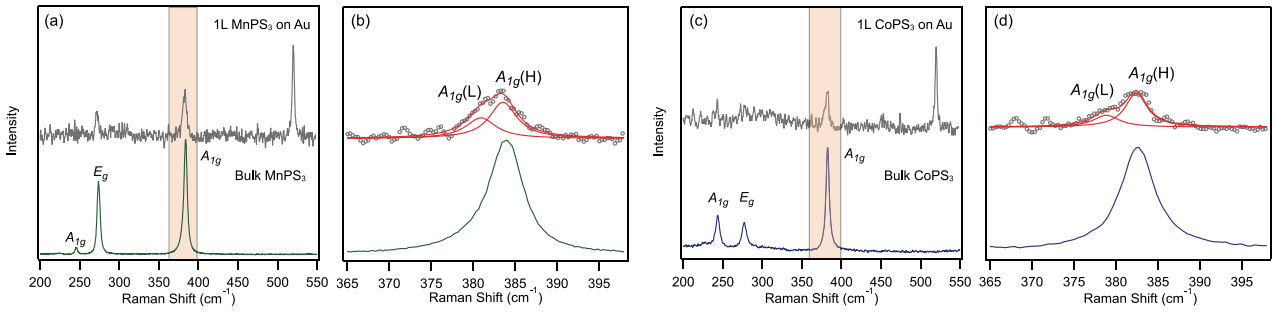

Fig. 5. Comparison of Raman spectra of (a) $MnPS_3$ and (c) $CoPS_3$ in monolayer and bulk obtained with a 532 nm laser at room temperature, and the zoom up of the A_{1g} peak for (b) $MnPS_3$ and (d) $CoPS_3$ at about 380 cm^{-1}. The red lines are the curves fitted to the monolayer Raman spectra using the Lorentz function.

used to assess the vibrational modes of both monolayer and bulk MPX_3 at room temperature. The Raman modes of MPX_3 family mainly derived from metal and ligand units with vibrational modes of the D_{3d} symmetry group [43]. As illustrated in Fig. 5, the in-plane E_g (275 cm^{-1}) and out-of-plane A_{1g} mode (248 and 384 cm^{-1}) can be identified in both monolayer and bulk, indicating the stability of monolayer MPX_3 in atmosphere conditions. The Si substrate is responsible for the additional peak at 520 cm^{-1} in the monolayer. At first glance, the Raman results of ultra-thin $CoPS_3$ and $MnPS_3$ exfoliated on Au substrate are similar to the previous spectra on the SiO_2 substrate, where the Raman vibrational modes remain almost constant from bulk to monolayer due to a weaker interlayer interaction compared to other 2D materials [44–46]. However, an anomalous feature is observed in the most prominent peak close to 380 cm^{-1}, where the typical A_{1g} mode of the P-S bond vibration splits into a high-frequency A_{1g}(H) and a low-frequency A_{1g}(L) component. The A_{1g}(H) modes for monolayer $MnPS_3$ and monolayer $CoPS_3$ exhibit slight position variation from the A_{1g} of the bulk, whereas the A_{1g}(L) component is significantly blue-shifted. The most probable explanation for the observed splitting and peak-shift is the Au substrate-induced strain or electron doping, which is consistent with the shift of the chemical state of the metal ions of ultra-thin samples observed in XPS. A similar phenomenon has been observed in 1L MoS_2 exfoliated on a Au substrate [47]. Therefore, the removal of the Au film, e.g. chemical etching with KI/I_2 solution, and the transfer of the 1L sample membrane onto an insulating substrate are important prerequisites for potential electronic applications or for further investigation of the intrinsic physical properties of the atomic layer MPX_3 [48].

4. Conclusions

In summary, Au-deposited substrates, after exposure to the atmosphere for more than one week, can be effectively reactivated through oxygen plasma treatment, enabling the preparation of large-area 2D MPX_3 flakes via mechanical exfoliation. Comparative analysis of Ar and O_2 plasma-treated results demonstrates that the cleanliness, smoothness, and adhesion properties of the substrate are critical for the successful acquisition of 2D flakes. The 2D flakes produced through this process were characterized using AFM, XPS, and Raman spectroscopy, which demonstrated that the monolayer and few-layer flakes are chemically and structurally stable. In addition, the interaction of Au/1L MPX_3 interface, which affects the vibrational properties and binding energy, has also been observed. The standard metal-assisted mechanical exfoliation methods need to be performed immediately after deposition due to the sensitivity of the substrate to air and the process is highly dependent on the deposition equipment and metal film growth procedure. However, the introduction of the gentle oxygen plasma treatment, as described above, effectively mitigates the issue of metal substrate failure caused by prolonged exposure to air and provides a post-treatment strategy to optimize the surface roughness of the grown Au substrate thereby improving the exfoliation efficiency and reducing the cost and requirements of the metal-assisted exfoliation process. We believe that our study constitutes an important step toward the further development of the metal-assisted exfoliation method and future 2D experimental research.

CRediT authorship contribution statement

Mouhui Yan: Writing – original draft, Methodology, Formal analysis, Data curation. **Haotian Wang:** Writing – review & editing, Resources, Data curation. **Guanghui Cao:** Writing – review & editing, Resources, Conceptualization. **Wei Ren:** Writing – review & editing, Supervision, Resources, Project administration, Conceptualization.

Declaration of competing interest

The authors declare that they have no known competing financial interests or personal relationships that could have appeared to influence the work reported in this paper.

Data availability

Data will be made available on request.

Acknowledgments

This work was supported by National Natural Science Foundation of China (Grants No. 52271007, No. 12074241, No. 12311530675, and No. 52130204), Science and Technology Commission of Shanghai Municipality, China (Grants No. 22XD1400900, No. 20501130600, No. 21JC1402700, No. 21JC1402600, and No. 22YF1413300). We thank Songshan Lake Materials Laboratory (No. XMYS2023002) for the experimental support of this work.

Appendix A. Supplementary materials

Supplementary material related to this article can be found online at https://doi.org/10.1016/j.cplett.2024.141634. The supplementary material contains the AFM characterization and exfoliation results of Au substrates after 9 min plasma treatment.

References

[1] R.F. Frindt, Superconductivity in ultrathin $NbSe_2$ layers, Phys. Rev. Lett. 28 (5) (1972) 299–301.
[2] K.S. Novoselov, A.K. Geim, S.V. Morozov, D. Jiang, Y. Zhang, S.V. Dubonos, I.V. Grigorieva, A.A. Firsov, Electric field effect in atomically thin carbon films, Science 306 (5696) (2004) 666–669.
[3] S. Das, J.A. Robinson, M. Dubey, H. Terrones, M. Terrones, Beyond graphene: Progress in novel two-dimensional materials and van der Waals solids, Annu. Rev. Mater. Res. 45 (1) (2015) 1–27.
[4] X. Wang, A.M. Jones, K.L. Seyler, V. Tran, Y. Jia, H. Zhao, H. Wang, L. Yang, X. Xu, F. Xia, Highly anisotropic and robust excitons in monolayer black phosphorus, Nat. Nanotechnol. 10 (6) (2015) 517–521.

[5] K. Zhang, Y. Feng, F. Wang, Z. Yang, J. Wang, Two dimensional hexagonal boron nitride (2D-hBN): synthesis, properties and applications, J. Mater. Chem. C 5 (46) (2017) 11992–12022.

[6] B. Anasori, M.R. Lukatskaya, Y. Gogotsi, 2D metal carbides and nitrides MXenes for energy storage, Nat. Rev. Mater. 2 (2) (2017) 16098.

[7] M.A. McGuire, H. Dixit, V.R. Cooper, B.C. Sales, Coupling of crystal structure and magnetism in the layered, ferromagnetic insulator CrI_3, Chem. Mater. 27 (2) (2015) 612–620.

[8] C. Gong, L. Li, Z. Li, H. Ji, A. Stern, Y. Xia, T. Cao, W. Bao, C. Wang, Y. Wang, Z.Q. Qiu, R.J. Cava, S.G. Louie, J. Xia, X. Zhang, Discovery of intrinsic ferromagnetism in two-dimensional van der Waals crystals, Nature 546 (7657) (2017) 265–269.

[9] T. Chowdhury, E.C. Sadler, T.J. Kempa, Progress and prospects in transition-metal dichalcogenide research beyond 2D, Chem. Rev. 120 (22) (2020) 12563–12591.

[10] D. Deng, K.S. Novoselov, Q. Fu, N. Zheng, Z. Tian, X. Bao, Catalysis with two-dimensional materials and their heterostructures, Nat. Nanotechnol. 11 (3) (2016) 218–230.

[11] S. He, J. He, W. Zhang, L. Zhao, D. Liu, X. Liu, D. Mou, Y.-B. Ou, Q.-Y. Wang, Z. Li, L. Wang, Y. Peng, Y. Liu, C. Chen, L. Yu, G. Liu, X. Dong, J. Zhang, C. Chen, Z. Xu, X. Chen, X. Ma, Q. Xue, X.J. Zhou, Phase diagram and electronic indication of high-temperature superconductivity at 65 K in single-layer FeSe films, Nature Mater. 12 (7) (2013) 605–610.

[12] Y. Xue, Q. Zhang, W. Wang, H. Cao, Q. Yang, L. Fu, Opening two-dimensional materials for energy conversion and storage: a concept, Adv. Energy Mater. 7 (19) (2017) 1602684.

[13] E.C. Ahn, 2D materials for spintronic devices, npj 2D Mater. Appl. 4 (1) (2020) 17.

[14] G.R. Bhimanapati, Z. Lin, V. Meunier, Y. Jung, J. Cha, S. Das, D. Xiao, Y. Son, M.S. Strano, V.R. Cooper, L. Liang, S.G. Louie, E. Ringe, W. Zhou, S.S. Kim, R.R. Naik, B.G. Sumpter, H. Terrones, F. Xia, Y. Wang, J. Zhu, D. Akinwande, N. Alem, J.A. Schuller, R.E. Schaak, M. Terrones, J.A. Robinson, Recent advances in two-dimensional materials beyond graphene, ACS Nano 9 (12) (2015) 11509–11539.

[15] D. Akinwande, C. Huyghebaert, C.-H. Wang, M.I. Serna, S. Goossens, L.-J. Li, H.-S.P. Wong, F.H.L. Koppens, Graphene and two-dimensional materials for silicon technology, Nature 573 (7775) (2019) 507–518.

[16] F. Wang, T.A. Shifa, P. Yu, P. He, Y. Liu, F. Wang, Z. Wang, X. Zhan, X. Lou, F. Xia, J. He, New frontiers on van der Waals layered metal phosphorous trichalcogenides, Adv. Funct. Mater. 28 (37) (2018) 1802151.

[17] R. Samal, G. Sanyal, B. Chakraborty, C.S. Rout, Two-dimensional transition metal phosphorous trichalcogenides MPX_3: a review on emerging trends, current state and future perspectives, J. Mater. Chem. A 9 (5) (2021) 2560–2591.

[18] A. Chaves, J.G. Azadani, H. Alsalman, D.R. Da Costa, R. Frisenda, A.J. Chaves, S.H. Song, Y.D. Kim, D. He, J. Zhou, A. Castellanos-Gomez, F.M. Peeters, Z. Liu, C.L. Hinkle, S.-H. Oh, P.D. Ye, S.J. Koester, Y.H. Lee, P. Avouris, X. Wang, T. Low, Bandgap engineering of two-dimensional semiconductor materials, npj 2D Mater. Appl. 4 (1) (2020) 29.

[19] S. Rahman, J.F. Torres, A.R. Khan, Y. Lu, Recent developments in van der Waals antiferromagnetic 2D materials: synthesis, characterization, and device implementation, ACS Nano 15 (11) (2021) 17175–17213.

[20] R. Kumar, R.N. Jenjeti, M.P. Austeria, S. Sampath, Bulk and few-layer $MnPS_3$: a new candidate for field effect transistors and UV photodetectors, J. Mater. Chem. C 7 (2) (2019) 324–329.

[21] Z. Cai, B. Liu, X. Zou, H.-M. Cheng, Chemical vapor deposition growth and applications of two-dimensional materials and their heterostructures, Chem. Rev. 118 (13) (2018) 6091–6133.

[22] J. Zhou, C. Zhu, Y. Zhou, J. Dong, P. Li, Z. Zhang, Z. Wang, Y.-C. Lin, J. Shi, R. Zhang, Y. Zheng, H. Yu, B. Tang, F. Liu, L. Wang, L. Liu, G.-B. Liu, W. Hu, Y. Gao, H. Yang, W. Gao, L. Lu, Y. Wang, K. Suenaga, G. Liu, F. Ding, Y. Yao, Z. Liu, Composition and phase engineering of metal chalcogenides and phosphorous chalcogenides, Nature Mater. 22 (4) (2023) 450–458.

[23] W. Bai, Z. Hu, C. Xiao, J. Guo, Z. Li, Y. Zou, X. Liu, J. Zhao, W. Tong, W. Yan, Z. Qu, B. Ye, Y. Xie, Parasitic ferromagnetism in few-layered transition-metal chalcogenophosphate, J. Am. Chem. Soc. 142 (24) (2020) 10849–10855.

[24] Y. Huang, E. Sutter, N.N. Shi, J. Zheng, T. Yang, D. Englund, H.-J. Gao, P. Sutter, Reliable exfoliation of large-area high-quality flakes of graphene and other two-dimensional materials, ACS Nano 9 (11) (2015) 10612–10620.

[25] P.Y. Huang, C.S. Ruiz-Vargas, A.M. Van Der Zande, W.S. Whitney, M.P. Levendorf, J.W. Kevek, S. Garg, J.S. Alden, C.J. Hustedt, Y. Zhu, J. Park, P.L. McEuen, D.A. Muller, Grains and grain boundaries in single-layer graphene atomic patchwork quilts, Nature 469 (7330) (2011) 389–392.

[26] X. Zhang, Y. Li, W. Mu, W. Bai, X. Sun, M. Zhao, Z. Zhang, F. Shan, Z. Yang, Advanced tape-exfoliated method for preparing large-area 2D monolayers: a review, 2D Mater. 8 (3) (2021) 032002.

[27] J. Shim, S.-H. Bae, W. Kong, D. Lee, K. Qiao, D. Nezich, Y.J. Park, R. Zhao, S. Sundaram, X. Li, H. Yeon, C. Choi, H. Kum, R. Yue, G. Zhou, Y. Ou, K. Lee, J. Moodera, X. Zhao, J.-H. Ahn, C. Hinkle, A. Ougazzaden, J. Kim, Controlled crack propagation for atomic precision handling of wafer-scale two-dimensional materials, Science 362 (6415) (2018) 665–670.

[28] Y. Huang, Y.-H. Pan, R. Yang, L.-H. Bao, L. Meng, H.-L. Luo, Y.-Q. Cai, G.-D. Liu, W.-J. Zhao, Z. Zhou, L.-M. Wu, Z.-L. Zhu, M. Huang, L.-W. Liu, L. Liu, P. Cheng, K.-H. Wu, S.-B. Tian, C.-Z. Gu, Y.-G. Shi, Y.-F. Guo, Z.G. Cheng, J.-P. Hu, L. Zhao, G.-H. Yang, E. Sutter, P. Sutter, Y.-L. Wang, W. Ji, X.-J. Zhou, H.-J. Gao, Universal mechanical exfoliation of large-area 2D crystals, Nature Commun. 11 (1) (2020) 2453.

[29] S.E. Panasci, E. Schilirò, G. Greco, M. Cannas, F.M. Gelardi, S. Agnello, F. Roccaforte, F. Giannazzo, Strain, doping, and electronic transport of large area monolayer MoS_2 exfoliated on gold and transferred to an insulating substrate, ACS Appl. Mater. Interfaces 13 (26) (2021) 31248–31259.

[30] M. Velický, G.E. Donnelly, W.R. Hendren, S. McFarland, D. Scullion, W.J.I. DeBenedetti, G.C. Correa, Y. Han, A.J. Wain, M.A. Hines, D.A. Muller, K.S. Novoselov, H.D. Abruña, R.M. Bowman, E.J.G. Santos, F. Huang, Mechanism of gold-assisted exfoliation of centimeter-sized transition-metal dichalcogenide monolayers, ACS Nano 12 (10) (2018) 10463–10472.

[31] Y. Jin, Y. Jin, K. Li, M. Yan, Y. Guo, Y. Zhou, A. Preobrajenski, Y. Dedkov, E. Voloshina, Mixed insulating state for van der Waals $CoPS_3$, J. Phys. Chem. Lett. 13 (45) (2022) 10486–10493.

[32] M. Yamamoto, T. Matsumae, Y. Kurashima, H. Takagi, T. Suga, T. Itoh, E. Higurashi, Comparison of argon and oxygen plasma treatments for ambient room-temperature wafer-scale Au–Au bonding using ultrathin Au films, Micromachines 10 (2) (2019) 119.

[33] M. Yamamoto, E. Higurashi, T. Suga, R. Sawada, T. Itoh, Properties of various plasma surface treatments for low-temperature Au–Au bonding, Japan. J. Appl. Phys. 57 (4S) (2018) 04FC12.

[34] K. Raiber, A. Terfort, C. Benndorf, N. Krings, H.-H. Strehblow, Removal of self-assembled monolayers of alkanethiolates on gold by plasma cleaning, Surf. Sci. 595 (1–3) (2005) 56–63.

[35] F. Liu, W. Wu, Y. Bai, S.H. Chae, Q. Li, J. Wang, J. Hone, X.-Y. Zhu, Disassembling 2D van der Waals crystals into macroscopic monolayers and reassembling into artificial lattices, Science 367 (6480) (2020) 903–906.

[36] K.-z. Du, X.-z. Wang, Y. Liu, P. Hu, M.I.B. Utama, C.K. Gan, Q. Xiong, C. Kloc, Weak van der Waals stacking, wide-range band gap, and Raman study on ultrathin layers of metal phosphorus trichalcogenides, ACS Nano 10 (2) (2016) 1738–1743.

[37] G.Z. Magda, J. Pető, G. Dobrik, C. Hwang, L.P. Biró, L. Tapasztó, Exfoliation of large-area transition metal chalcogenide single layers, Sci. Rep. 5 (1) (2015) 14714.

[38] E. Voloshina, Y. Jin, Y. Dedkov, ARPES studies of the ground state electronic properties of the van der Waals transition metal trichalcogenide $CoPS_3$, Chem. Phys. Lett. 823 (2023) 140511.

[39] L. Zhong, H. Chen, W. Xie, W. Jia, Y. Xiao, B. Cheng, L. Lin, S. Lei, Intercalation and defect engineering of layered $MnPS_3$ for greatly enhanced capacity and stability in sodium-ion batteries, Chem. Eng. J. 481 (2024) 148370.

[40] M.A. Van Veenendaal, G.A. Sawatzky, Nonlocal screening effects in 2*p* x-ray photoemission spectroscopy core-level line shapes of transition metal compounds, Phys. Rev. Lett. 70 (16) (1993) 2459–2462.

[41] Z.-X. Shen, J.W. Allen, P.A.P. Lindberg, D.S. Dessau, B.O. Wells, A. Borg, W. Ellis, J.S. Kang, S.-J. Oh, I. Lindau, W.E. Spicer, Photoemission study of CoO, Phys. Rev. B 42 (3) (1990) 1817–1828.

[42] M. Velický, A. Rodriguez, M. Bouša, A.V. Krayev, M. Vondráček, J. Honolka, M. Ahmadi, G.E. Donnelly, F. Huang, H.D. Abruña, K.S. Novoselov, O. Frank, Strain and charge doping fingerprints of the strong interaction between monolayer MoS_2 and gold, J. Phys. Chem. Lett. 11 (15) (2020) 6112–6118.

[43] A. Hashemi, H.-P. Komsa, M. Puska, A.V. Krasheninnikov, Vibrational properties of metal phosphorus trichalcogenides from first-principles calculations, J. Phys. Chem. C 121 (48) (2017) 27207–27217.

[44] Y.-J. Sun, Q.-H. Tan, X.-L. Liu, Y.-F. Gao, J. Zhang, Probing the magnetic ordering of antiferromagnetic $MnPS_3$ by raman spectroscopy, J. Phys. Chem. Lett. 10 (11) (2019) 3087–3093.

[45] Q. Liu, L. Wang, Y. Fu, X. Zhang, L. Huang, H. Su, J. Lin, X. Chen, D. Yu, X. Cui, J.-W. Mei, J.-F. Dai, Magnetic order in XY-type antiferromagnetic monolayer $CoPS_3$ revealed by Raman spectroscopy, Phys. Rev. B 103 (23) (2021) 235411.

[46] C. Lee, H. Yan, L.E. Brus, T.F. Heinz, J. Hone, S. Ryu, Anomalous lattice vibrations of single- and few-layer MoS_2, ACS Nano 4 (5) (2010) 2695–2700.

[47] E. Pollmann, S. Sleziona, T. Foller, U. Hagemann, C. Gorynski, O. Petri, L. Madauß, L. Breuer, M. Schleberger, Large-area, two-dimensional MoS_2 exfoliated on gold: Direct experimental access to the metal–semiconductor interface, ACS Omega 6 (24) (2021) 15929–15939.

[48] S.E. Panasci, E. Schilirò, F. Migliore, M. Cannas, F.M. Gelardi, F. Roccaforte, F. Giannazzo, S. Agnello, Substrate impact on the thickness dependence of vibrational and optical properties of large area MoS_2 produced by gold-assisted exfoliation, Appl. Phys. Lett. 119 (9) (2021) 093103.